Review article

Tian Zhong* and Philippe Goldner

Emerging rare-earth doped material platforms for quantum nanophotonics

Abstract: Rare-earth dopants are arguably one of the most studied optical centers in solids, with applications spanning from laser optoelectronics, biosensing, lighting to displays. Nevertheless, harnessing rare-earth dopants' extraordinary coherence properties for quantum information technologies is a relatively new endeavor, and has been rapidly advancing in recent years. Leveraging the state-of-the-art photonic technologies, on-chip rare-earth quantum devices functioning as quantum memories, single photon sources and transducers have emerged, often with potential performances unrivaled by other solid-state quantum technologies. These existing quantum devices, however, nearly exclusively rely on macroscopic bulk materials as substrates, which may limit future scalability and functionalities of such quantum systems. Thus, the development of new platforms beyond single crystal bulk materials has become an interesting approach. In this review article, we summarize the latest progress towards nanoscale, low-dimensional rare-earth doped materials for enabling next generation rare-earth quantum devices. Different platforms with a variety of synthesis methods are surveyed. Their key metrics measured to date are presented and compared. Special attention is placed on the connection between the topology of each platform to its target device applications. Lastly, an outlook for near term prospects of these platforms are given, with a hope to spur broader interests in rare-earth doped materials as a promising candidate for quantum information technologies.

Keywords: rare-earth ions; coherent quantum material; nanophotonics; nanocrystals; hybrid quantum material.

*Corresponding author: Tian Zhong, Pritzker School of Molecular Engineering, University of Chicago, Chicago, IL 60637, USA, e-mail: tzh@uchicago.edu. https://orcid.org/0000-0003-3884-7453
Philippe Goldner: Institut de Recherche de Chimie Paris, PSL University, Chimie ParisTech, CNRS, 11 rue Pierre et Marie Curie, 75005 Paris, France

1 Introduction

Solid-state quantum nanophotonics has emerged as one of the most active fields in quantum engineering [1]. In particular, optically active atomic or atom-like defects in solids that simultaneously possess long-lived spin coherence and stable optical transitions play key roles in the development of quantum networks [2–4], quantum sensing [5] and quantum information processing [6–8]. Among numerous candidates, rare-earth doped materials have attracted significant interests in recent years, and are rapidly advancing. The emergent field of rare-earth nanophotonics inherits the rich history of rare-earth spectroscopy [9, 10], and leverages the cutting-edge nanophotonic technologies to enable a new class of devices that are highly coherent, efficient and scalable. These devices include optical memories [11, 12], photon sources [13, 14] and optical-microwave transducers [15, 16]. At the heart of this development is the fundamental science and engineering of rare-earth doped materials with a wide variety of chemical compositions, physical behaviors, topologies, and synthesis methods. The rich library of material properties offers nearly unlimited opportunities for quantum device engineering. At the same time, crucial device metrics also dictate the best combination of material topologies and growth techniques to achieve those specifications.

This connection between material growth and quantum device engineering is important to guide the rare-earth material design and synthesis. After decades of arduous efforts in perfecting bulk, single crystal hosts, newer platforms based on rare-earth doped nanocrystals, polycrystalline ceramics, and films tailored for quantum technologies have been gaining momentum and are begining to reap promising results. In this article, we summarize some of the most recent developments in emerging material platforms beyond bulk crystals for building the next generation rare-earth quantum photonic devices. We attempt to establish a common ground for material chemists, spectroscopists and device engineers in this field by highlighting the relationship between material metrics and device designs. The hope is to spur further

research in fundamental material science to understand, control and design better materials to meet the needs of fast-growing rare-earth quantum technologies. It should be pointed out that we do not intend to give a thorough review on rare-earth doped bulk crystals, nor the spectroscopic techniques used to characterize them. A number of comphrehensive reviews on those topics are already available to interested readers [9, 10, 17–19], and will not be repeated here. We stress that research on bulk crystals has played a key role in driving rare-earth quantum technologies and will continue to propel advancement of this field. This paper, on the other hand, aims to inform readers about some of the new rare-earth material platforms that have potential advantages over conventional bulk materials.

This article is organized as follows: Section 2 gives a review of rare-earth quantum photonic devices developed to date and highlights the trend in underlying material platforms. Section 3 surveys in more detail the progress in several emerging material platforms. In Section 4, we give an outlook for future material development and elaborate several key metrics needed to be accomplished in order to push forward the field of rare-earth nanophotonics.

2 Rare-earth quantum photonic materials and devices

Rare-earth elements include lanthanides, scandium and yttrium. They are common dopants in host crystals such as yttrium aluminum garnet ($Y_3Al_5O_{12}$ or YAG), Y_2SiO_5 (YSO), Y_2O_3, or YVO_4 (YVO). The 4f shell of rare-earth ions in crystals is partially occupied and is shielded from the interaction with the crystalline environment by 5s and 5p outer shells. The 4f electrons are highly localized and the 4f–4f intra-shell transitions are parity-forbidden in free space, but become weakly allowed in the presence of a crystal field, which results in sharp optical transitions with high quantum efficiency. Sharp optical transitions (equivalent quality factor over 10^{11}) at cryogenic temperatures are correlated with long optical T_1 lifetimes (hundreds of μs to ms) but also weak oscillator strengths. Electronic Zeeman and hyperfine transitions in the radio-frequency or microwave regimes are abundant. When doped into a YSO host with small nuclear magnetic moments, record long spin coherence times – 6 h in Eu:YSO [20] at 2 K and 1.3 s in Er:YSO [21] at 1.4 K – have been achieved. Such long coherence times combined with a rich selection of spin levels (both electronic and nuclear) and optical addressability make rare-earth ions attractive candidates for qubits as

a building block in quantum information science. Furthermore, optical transitions exhibit inhomogeneous broadenings that are typically 10^{5-6} times the homogeneous linewidths, indicating an excellent prospect for dense spectral multiplexing of qubits or memories to enable large data processing and storage bandwidths [22, 23].

One of the most successful applications of rare-earth doped crystals in quantum technology is optical quantum memories. These memories – which faithfully store a qubit encoded on a single photon – have performances unmatched by other solid-state systems including nitrogen-vacancies in diamonds and semiconductor quantum dots. For reviews on rare-earth quantum memories, readers are referred to [11, 12]. Landmark ensemble experiments include storage of light up to a minute using electromagnetically induced transparency (EIT) in praseodymium doped yttrium orthosilicate (Pr^{3+}:YSO) [24, 25], quantum storage of photonic entanglement in neodymium (Nd) doped YSO (Nd^{3+}:YSO) [26, 27] and thulium-doped lithium niobate waveguides [28], optical memory at the single photon level in Nd doped yttrium orthovanadate (Nd:YVO) [29–31] and quantum level spin storage in Eu^{3+}:YSO [32], conditional phase shifts between two ensembles of europium (Eu) in YSO [33], up to 69% efficient quantum memory for light in Pr^{3+}:YSO [34–36], and a quantum optical connection between a cold atomic gas and Pr^{3+} in YSO [37]. These ensemble-based memories provide natural interfaces between optical photons and spins at radio-frequency or microwave regimes, which can also be harnessed to realize quantum transducers interconnecting distant superconducting quantum circuits. Hybrid quantum systems based on rare-earth ensembles see the opportunities in microwave quantum storage [38] and microwave-to-optical conversion [15, 16]. To date, high cooperativity coupling of rare-earth spins to a superconducting resonator has been demonstrated [39, 40]. Unit efficiency microwave to optical conversion via magneto-optic coupling has been proposed [16], and its experimental implementation is being pursued [41–43].

Ultimately, the most powerful rare-earth quantum technologies will be devices operating on invidividual ions [13, 14, 44, 45]. To that end, optical addressing of single ions is coming into focus. The progress, however, has been hindered by the long optical lifetimes of rare-earth ions and resultant faint photoluminescence. So far, only a few experiments have succeeded in isolating individual praseodymium [46–48], cerium [49–51], neodymium [13] and erbium [14, 52] ions. It is worth noting that majority of these experiments were not probing ions via their highly coherent but weak 4f–4f optical transitions. Taking Pr and Ce as examples, bright 4f–5d transitions from high lying electronic

levels were exploited to enhance the detection sensitivity of individual ions, although these transitions typically have low radiative efficiencies in the zero-phonon lines. To directly access the 4f–4f transitions of single ions, the emission rate of individual emitters need to be enhanced. Recent works [13, 14] have been successful in achieving this by coupling ions to nanophotonic cavities with sub-wavelength scale dimensions (more discussions on cavities in the next paragraph). Both experiments achieved Purcell enhancement of ions' emission on the order of hundreds, allowing direct optical detection of individual ions with sufficient signal-to-noise performance using state-of-the-art superconducting nanowire detector technology. These results point to a viable approach to efficiently detect and coherently control individual ions in an on-chip nanophotonic platform.

The weak oscillator strengths of rare-earth emitters require significant enhancement of their atomic absorption cross-sections in order to strongly interact with light at the quantum level. One effective way to achieve such enhancement is to modify the local photonic density of states using nanophotonic structures including waveguides and cavities. Rare-earth doped photonic waveguides have been realized by ion-indiffusion in Tm or Er doped $LiNbO_3$ [28, 53, 54], laser written channels in Pr:YSO crystals [55], and high-index membranes deposited or transferred on top of doped oxide substrates [14, 56–58]. These waveguides provide transverse confinement of the optical field interacting with dopants, thus enhancing the coupling strengths. In the case of ion-indiffused and laser written devices, the rare-earth emitters align with the peak field intensity in the waveguide, whereas in systems based on high-index materials placed on top of doped crystals, the optical field evanescently couples to the dopants near the material interfaces. All of these designs have demonstrated enhanced light-matter interactions, and preserved optical coherence of the dopants comparable to bulk crystal hosts. The long coherence despite the fabrication processes highlights the remarkable robustness of rare-earth quantum emitters. The waveguide scheme has also been extended to cavities by forming a micro-ring [57, 58] or patterning photonic crystal lattices [14] along the waveguide. For cavity-based systems, an important figure of merit is the Q/V ratio where Q is the quality factor and V is the normalized mode volume of the cavity in a unit of $(\lambda/n)^3$ [44]. Focused ion beam-milled photonic crystal nanobeam resonators achieving Q/V in the order of 10^4 have been fabricated [59, 60], which enabled first nanophotonic quantum memories [31, 61] based on a mesoscopic ensemble of dopants and coherent optical addressing of individual ions. The photonic crystal cavities were proven effective to strongly enhance the spontaneous emission rate of rare-earth ions via the Purcell effect [13, 14]. When the enhancement is sufficiently large compared to other optical dephasing processes, radiatively-limited single photon emission from individual ions becomes feasible and has been demonstrated recently [13]. Besides waveguides and cavities, other techniques for controlling the rare-earth emission rate were also proposed. One example is a hybrid scheme in which the rare-earths are coupled to highly optically absorbing materials such as graphene via near field interactions [62].

3 Recent progress towards low-dimensional rare-earth doped materials

The majority of rare-earth quantum photonic devices demonstrated to date have been based on bulk, single crystal doped materials (an example is shown in Figure 1A). These macroscopic bulk matrices, while having superb crystalline qualities, remain difficult to grow and lack some prospects for scalable fabrication desired by future quantum technologies. Perhaps the most scalable platforms for on-chip device integration are submicron thick membranes (Figure 1C), on which large arrays of devices can be lithographically patterned and etched. High quality thin membranes of rare-earth doped materials have not been commonly available due to their complicated chemical compositions and difficult growth processes. The most promising synthesis methods so far are atomic layer deposition and molecular beam epitaxy, the latest development of which will be discussed in the next section. Another class of doped materials that are promising for nanophotonic applications are nanocrystal and polycrystalline ceramics (Figure 1B). These powder-form materials, have gained significant traction due to recent reports of long coherence even though the size of these nanocrystals is as small as 60 nm [64]. The rare-earth doped nanocrystals are promising systems for single ion detection and control as they minimize background signals and can allow for higher Rabi frequencies in microscopy setups [46, 47, 64]. They can also be inserted into high quality factor micro-cavities to enhance light-atom interactions, increasing emission rates through the Purcell effect and collection efficiencies [65]. Perhaps the biggest advantage of nanocrystals is their relatively easy synthesis methods. Compared to single crystal bulk materials or epitaxial films, many nanocrystals can be grown with commercially available raw materials and in-house processing capabilities. Once developed,
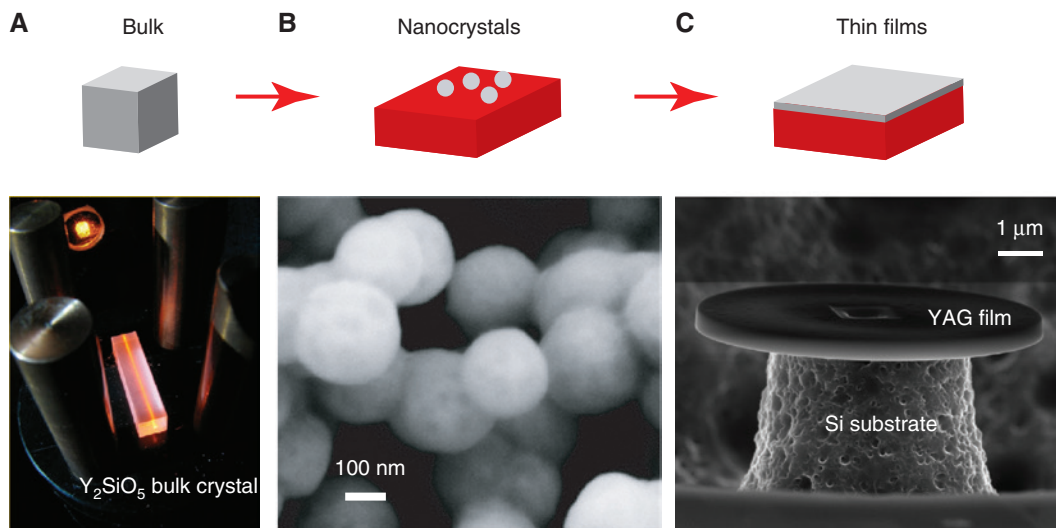
Figure 1: Evolving material platforms for rare-earth quantum devices from (A) macroscopic bulk crystals (reprinted from [11]) to low-dimensional materials including (B) doped nanocrystals (reprinted from [63]) and (C) sub-micron thick YAG films fabricated by smart-cut and thermal exfoliation (unpublished work from T. Zhong).

the rare-earth doped nanocrystals can find widespread adoption as practical quantum technologies for sensing and communications.

3.1 Nanoparticles and thin films

3.1.1 Nanocrystals and polycrystalline ceramic materials

A first approach to obtain these materials is to use chemical methods, the so-called bottom-up strategy. This has been first used to produce Eu^{3+}:Y_2O_3 micro-size particles with 60 nm crystalline domains by a solvothermal method [64, 66]. These particles, as most of those studied so far by high-resolution and coherent spectroscopy, are polycrystalline, i.e. each particle is made of several crystallites. Optical properties were determined on samples in the form of a powder. Photon echoes, well known for providing an accurate measurement of homogeneous linewidths in transparent materials [67, 68], can also be observed in powders that strongly scatter light as first demonstrated by Beaudoux et al. [69] and recently theoretically analyzed [70]. Application of this technique to the above particles led to a homogeneous linewidth for Eu^{3+} $^7F_0 \rightarrow {}^5D_0$ transition at 581 nm of 86 kHz at 1.3 K [64]. This was about one to two orders of magnitude lower than previous results obtained on Eu:Y_2O_3 nanocrystals [71]. It is however, much larger than values obtained in the best single crystals (600 Hz [72]) or transparent ceramics (3.5 kHz) [73], although it shoud be noted that considerable dispersion of linewidths is found in single crystals grown by different

methods [74]. Non-yttrium based nanoparticles such as $CaWO_4$ have also been studied extensively [75–77]. The absence of yttrium nuclear spin baths in the $CaWO_4$ host may provide advantages in the coherence properties of rare-earth dopants, but this needs to be verified by further coherent spectroscopic measurements.

Light scattering by particles introduces losses that are very detrimental to cavities quality factor, and should be minimized. The particle diameter d is a major factor to consider since the scattering cross-section varies as d^6 [65]. Moreover, to be able to use isolated particles, aggregation should be avoided. This was made possible using homogeneous precipitation, a technique that led to low particle size dispersion and spherical shapes [78]. To obtain Y_2O_3 cubic phase, high temperature annealing of the precursor hydrocarbonates particles is required. It was shown that treatment at 1200 °C reduced inhomogeneous linewidths down to ≈10 GHz for 0.5% Eu^{3+} doping, a value comparable to bulk ones [79]. This was observed for particle and crystallite sizes in the ranges 150–540 nm and 90–120 nm, respectively, suggesting that the decrease in linewidths was due to a decrease in defects, such as oxygen vacancies, in the volume of the nanocrystals. On particles of 400 nm diameter (130 nm crystallite diameter), an extensive study of homogeneous linewidths Γ_h as a function of temperature, magnetic field and time was performed by two and three-pulse photon echoes and spectral holeburning [80]. A surprising result was that magnetic fields up to 2.5 T had no effect on Γ_h, suggesting that dephasing from magnetic defects or impurities was not the main contribution to Γ_h. Indeed, it

was concluded that for temperatures < 12 K, Γ_h was due to interactions with two-level systems (TLS) and a temperature independent dephasing. While TLS effect has been previously identified in Y_2O_3 bulk crystals and nanoparticles [64, 74], it was not the case for the latter process. Based on a simple model, it was suggested that fluctuations in surface charges' number and positions lead to electric field noise that couples to rare-earth optical transitions through the Stark effect and therefore causes dephasing [80]. A similar mechanism was observed for the spin transitions of near-surface NV^- centers in diamonds [81]. Importantly, no sign of interaction between Eu^{3+} and a modified phonon density of states, related to the crystallite sizes [71], was observed. This indicates that there is no intrinsic size-related contribution, which would be very difficult to overcome, to the homogeneous linewidth of the studied particles. The narrowest homogeneous linewidths reported were 45 kHz at 1.3 K with a broadening of ≈100 kHz over 1 s [80]. Narrow linewidths were also demonstrated in smaller particles. Because of the required high temperature annealing that promotes sintering, it can be challenging to directly obtain small particles that stay non-aggregated. An alternative approach was proposed in which large particles are reduced in size by wet chemical etching in a weak acid. Starting from dispersed and well-crystallized particles of 450 nm diameter, particles down to 150 nm were obtained showing homogeneous linewidths of 34 kHz at 1.4 K, the smallest value reported so far for a nano-material [82]. The limited broadening induced by etching (≈10 kHz), while the particle size is reduced by 65% but the crystallite size remains unchanged, suggests that the latter is the relevant parameter for dephasing processes (Figure 2).
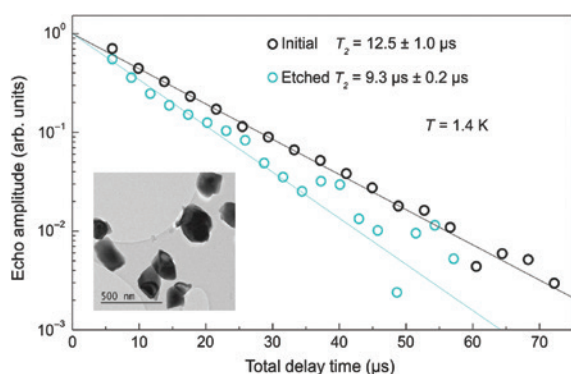
This was further supported by showing that etching proceeds by opening grain boundaries between crystallites in the particles. Single crystalline particles can therefore be produced, which may be useful when, for instance, a magnetic field should be applied in a specific direction or well defined Rabi frequencies are needed.

To assert the potential of rare-earth doped nanoparticles as quantum memories or processors, it is necessary to measure spin coherence lifetimes T_2, as qubits are usually defined within the energy level structure of ground state spins [83]. This was performed on 400 nm Eu^{3+}:Y_2O_3 particles using an all-optical technique for spin coherence manipulation and spin echo detection [84–86]. Powders cooled to 5 K showed nuclear spin echo signals for $^{151}Eu^{3+}$ with signal to noise ratio of about 10, proving that the technique actually works in a scattering medium, and sufficient for T_2 measurements [87]. Spin coherence lifetimes of 1.3 ms were recorded, increasing to about 3 ms under a 9 mT magnetic field (Figure 3). These values, one order of magnitude lower than in transparent ceramics [88] but still the longest reported for any nanoparticle with optically addressable spins, provide valuable insight into dephasing mechanisms. First, the strong dependance of T_2 for very weak magnetic field suggests that the main dephasing is due to a magnetic dipole-dipole interaction with electron spins carried by defects or impurities. Indeed, when the Zeeman interactions become larger than the dipole-dipole interaction, the effect of the latter is reduced. This magnetic noise also affects the optical transition, which can be expected to broaden to a similar level than the spin transition, i.e. ≈250 Hz, based on the excited and ground state gyromagnetic ratios in other hosts [89–91]. This is too small to account for the optical linewidth
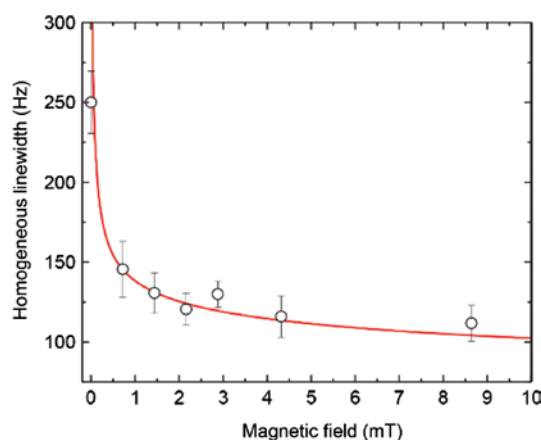

Figure 2: Optical echo decays in Eu^{3+}:Y_2O_3 nanoparticles before and after chemical etching.
Despite the size reduction from 450 nm to 150 nm, only limited broadening (≈10 kHz) is observed. Inset: 200 nm etched particles. Reproduced from [82] with permission from the Royal Society of Chemistry.

Figure 3: Nuclear spin homogeneous linewidth of $^{151}Eu^{3+}$:Y_2O_3 ($\pm 1/2 \rightarrow \pm 3/2$ ground state transition) in Y_2O_3 nanoparticles as a function of external magnetic field.
Reproduced from [87], CC-BY-4.0.

of 45 kHz, and supports the hypothesis of electric field perturbations as the main optical dephasing process. This is also in agreement with Stark coefficient of the optical transition [92] being 4–5 orders of magnitude larger than the spin one [93]. Coherent spin control was further demonstrated by an all-optical dynamical decoupling (DD) technique that resulted in T_2 up to 8 ms, limited by disorder and light scattering in the powders that prevent pulses with the accurate area to be applied [87]. This highlights the interest of using single particles with single crystalline structure for optimal decoherence control. It was also shown that spin state is well preserved in echo and DD sequences, which is a requirement for quantum storage. Apart from experiments on powders, spectroscopy of single Eu^{3+}:Y_2O_3 nanoparticles has been studied using a fiber micro-cavity [65]. In this setup, the particles are placed on a flat mirror which faces a concave profile laser-machined in an optical fiber. It was found that Eu^{3+} in 90 nm particles had inhomogeneous linewidths identical to what had been measured on powders, and that the cavity allowed detecting about 10 ions taking advantage of the Purcell effect.

Similar results have also been reported in Pr^{3+}:Y_2O_3 nanoparticles [94], obtained by homogeneous precipitation, for optical and spin transitions. Compared to Eu^{3+}, Pr^{3+} has generally stronger optical transitions and more favorable branching ratios that could be beneficial for coupling to a cavity. Hyperfine splittings are however, smaller [17], which limits the minimal pulse duration that can be applied to a specific transition between hyperfine levels and therefore operation fidelity. Homogeneous linewidths of between 100 and 300 kHz were observed for the $^3H_4 \rightarrow {}^1D_2$ transition at 619 nm and particles between 400 and 150 nm (crystallite size 120 and 80 nm). Interestingly, spin coherence lifetimes reached nearly 1 ms, longer than reported so far in bulk Pr^{3+} doped crystals, like YSO [95, 96]. This could be explained by lower gyromagnetic ratios for Pr^{3+} in Y_2O_3 according to calculations based on crystal field modeling of electronic levels [97, 98].

Pioneering experiments on high resolution spectroscopy of rare earth doped nanomaterials used a top-down approach, laser ablation, to produce Y_2O_3 nano-crystals with a monoclinic phase [71, 99]. Spectral hole burning was used to probe Eu^{3+} homogeneous linewidths, which were found in the several MHz range for crystals of 10 s of nm, likely to be highly agglomerated. Interactions with modified phonon density of states were proposed to explain the broadening.

Other top-down approaches have also been investigated, in which a single crystal is ground to nanoparticles. In Pr^{3+}:YSO, optical homogeneous linewidths of a few MHz

for single ions were reported for particles between 100 s of nm and a few microns, as well as spectral diffusion of 10 MHz over minutes for the larger particles [47, 100]. Strain induced by grinding and associated TLS could be the source of this significant broadening compared to the 80 kHz linewidth in the bulk crystal. Such mechanisms were also put forward in studies on Tm^{3+} doped YAG crystals ground to micron size powders and probed by spectral hole burning [101]. The main effect of strain was observed on spectral hole lifetimes that are significantly shortened under milling (several hours down to 10 s of minutes) and could be partially recovered with high-temperature annealing. Homogeneous linewidths, that can be estimated from hole widths, followed the same trends although the already broad values of several MHz for bulk crystals do not allow studying very narrow linewidths. Milled, micron-size powders of Er^{3+}:$LiNbO_3$ were studied by spectral hole burning and photon echoes, and showed that even low energy milling impacts kHz range homogeneous linewidths [102]. For powders with 1–100 μm crystals, annealing was able to recover close to bulk properties.

Another class of polycrystalline materials are transparent ceramics, which are usually obtained by sintering cubic phase nanoparticles under high temperature and high isostatic pressure (HIP). This results in the growth of micron size crystals with random orientations and a strong decrease of the material porosity, ultimately leading to negligible scattering losses [103]. Thanks to their high flexibility in composition, shape, and ability to build composite materials, transparent ceramics are thus an alternative to single crystals in a variety of photonic applications like lasers or scintillators, and could also allow obtaining new high performance materials in quantum technologies [104–106]. Eu^{3+} in Y_2O_3 transparent ceramic properties have been investigated in detail, as a function of doping concentration, post-synthesis treatment and co-doping with sintering aids. Optical transition inhomogeneous linewidths down to 9 GHz were observed for 1000 ppm Eu^{3+} doping [106, 107], comparable to bulk values, while co-doping with Zr^{4+} (5000 ppm), a common sintering aid, increased the linewidth to 100 GHz [108]. Homogeneous linewidths were also studied as a function of temperature, magnetic field and delay in three pulse experiments to reveal spectral diffusion processes [73]. This revealed complex behaviors, that could be in some cases analyzed by taking into account the dependence of perturbation correlation times on temperature and magnetic field. The narrowest homogeneous lines were 3.2 kHz for ceramics post-annealed in air and are due to several contributions, including TLS and possibly magnetic perturbations.

Dephasing was more pronounced in samples without post-annealing, underlining the role of oxygen in controlling defects' concentration and nature. This was further investigated by comparing high resolution spectroscopy with photoluminescence, electron paramagnetic resonance and thermo-luminescence, showing that defects related to oxygen vacancies, like F centers, seem to be correlated with optical linewidth [108]. Nuclear spin properties of $^{151}Eu^{3+}$ and $^{153}Eu^{3+}$ were also measured by the all-optical technique described above and showed remarkably long coherence lifetimes, up to 16 ms under a 3 mT magnetic field [88], close to values measured in $Eu^{3+}:Y_2SiO_5$ single crystal [109, 110]. As in the nanoparticles, spin transitions are much less sensitive to perturbations than optical transitions, pointing to a possible role of electric noise.

Very narrow inhomogeneous lines, as low as 442 MHz, have also be observed in Er^{3+} in Y_2O_3 transparent ceramics. This indicates a very high crystalline quality of the samples. Homogeneous linewidths measured at 2.5 K and under 0.65 T magnetic field vary between 10 and 50 kHz, depending on Er^{3+} concentration. In the case of paramagnetic ions, interaction between ground state spins themselves can cause strong dephasing, which can explain the observed dependence on Er^{3+} concentration [111]. At low Er^{3+} concentration, temperature dependence of Γ_h under magnetic field suggests that TLS contribution dominates the homogeneous linewidth. This suggests a low concentration in defects or impurities carrying electron spins, that could induce significant broadening by coupling to Er^{3+} electron spin.

3.1.2 Rare-earth doped films

Atomic layer deposition (ALD) is a common technique for obtaining Y_2O_3 films with well-controlled thickness and good crystalline quality [112]. A study of Eu^{3+} and Er^{3+} doped ALD films in the context of applications in quantum technologies was reported [113]. It showed that optimized growth followed by high temperature annealing resulted in Eu^{3+} luminescence spectra corresponding mainly to the Y_2O_3 cubic phase. In a 100 nm thick sample doped with 5% Eu^{3+} and deposited on (100) silicon wafers, $^5D_0$ level lifetimes reached 0.8 ms, close to bulk values. The $^7F_0 \rightarrow {}^5D_0$ inhomogeneous linewidth was about 200 GHz, a factor of 2 larger than expected from studies on transparent ceramics [107]. This could be due to stress in the film induced by differences in thermal expansion coefficients between silicon and Y_2O_3, which would also explain the shift of the line with the annealing temperature. It may also stem from the presence of defects

at grain boundaries as grain size in such polycrystalline thin films is of the order of 30 nm. $Eu^{3+}:Y_2O_3$ thin films with 3 μm thickness have also been obtained by chemical vapor deposition (CVD) on a sapphire substrate [114]. Inhomogeneous linewidth of 90 GHz was recorded for a doping level of 2%, about a factor of 2 larger compared to expected values in bulk materials. Spectral holeburning was used to determine homogeneous linewidths, which reached 1.2 MHz at 1.4 K. The broadening was attributed to TLS induced by disorder in the film. Ultra-thin films, which are of interest for dopant localization and hybrid devices [62], have also been investigated [113]. In films as thin as 7 nm, Er^{3+} luminescence at 1.5 μm showed decay times of about 1.5 ms, a long value for Er^{3+} nanomaterials, although still shorter than the 8.5 ms of bulk $Er^{3+}:Y_2O_3$. Further studies on coherent properties are needed to assert the potential of these systems for quantum technologies, which may require specific setups such as waveguides to deal with film/substrate geometries and the low number of active ions in very thin layers [56]. The simple chemical composition and stable cubic phase of Y_2O_3 make it possible to grow wafer-scale, epitaxial thin films. Indeed, single crystal, epitaxial Y_2O_3 have been synthesized using molecular beam epitaxy (MBE) on silicon wafers for high-k dielectric gate in MOSFET [115, 116]. Recently, this process has been improved to achieve exceptional qualities of Y_2O_3 films doped with Er^{3+} [117]. Controls of doping concentrations in the range of 1–100 parts per millions can be achieved. The thickness of the film up to 1.5 μm is also controllable with a precision down to a monolayer of dopants. The growth occurs via a two-dimensional (2D) layer-by-layer growth mode, resulting in smooth, uniform films. The surface roughness of the Y_2O_3 film was measured to be ≤0.6 nm r.m.s. The epitaxial host offers several distinct advantages: first, the single crystal film has significantly less optical loss and suggests better coherence for dopants; second, it allows atomic precision placement of rare-earth dopants via "delta-doping"; third, the wafer-size film allows scalable top-down device patterning using standard lithography and etching techniques. The photoluminescence of Er^{3+} was measured and shown in Figure 4A, which clearly showed two distinct transitions corresponding to two crystal symmetry sites: C_2 site at 1532 nm and C_{3i} at 1542 nm. The wavelengths of the peaks agree with those in bulk $Er^{3+}:Y_2O_3$ [118], confirming the correct Y site occupancies. Optical lifetimes and ground-state electron paramagnetic resonance were measured [117]. The photoluminescence decay gives a T_1 of 8.7 ms for C_2 site (Figure 4B), in excellent agreement with bulk $Er^{3+}:Y_2O_3$ measurement [118]. Optical and spin coherence are next
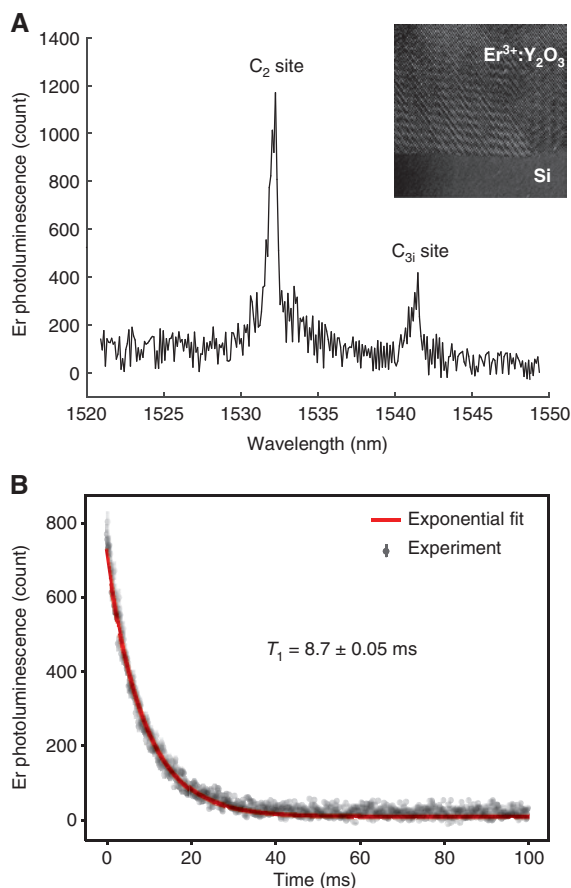
Figure 4: Photoluminescence of Er^{3+} in an epitaxial Y_2O_3 film grown on silicon using molecular beam epitaxy.
(A) Two $^4I_{13/2}-^4I_{15/2}$ optical transitions of Er confirm the correct crystal symmetry site occupancy. The inset shows a transmission electron microscope image of the Y_2O_3 lattice on silicon. (B) Measured optical lifetime of Er in C_2 site.

steps to fully characterize this epitaxial film material. Table 1 below summarizes different nanocrystals and thin film Y_2O_3 along with their spectroscopic properties measured to date. Besides Y_2O_3, other rare-earth doped films such as CaF_2 [119] and $CaWO_4$ phosphor [120] films have been synthesized, using MBE and Pechini sol-gel process, respectively. Holeburning and luminescent properties of rare-earth dopants in these films have been measured to show promising properties.

3.2 Other platforms

Other hybrid architectures have been considered, based on thin films or nanoparticles. A first example is the electrical control of coupling between rare-earth ions and a graphene layer [62]. Depending on the Fermi level in graphene, rare-earths can decay through photon emission, non-radiatively by creation of electron-hole pairs in the graphene layer or by excitation of graphene plasmons. This process however is only efficient at distances below 10 nm and is therefore maximized for very thin rare-earth doped films. This effect was observed in a $Er^{3+}:Y_2O_3$ thin film of about 60 nm thickness obtained by the metal organic decomposition method on an Si substrate [121]. A graphene layer was placed on top of the film and covered by a transparent solid polymer electrolyte to allow tuning of graphene Fermi level by a gate voltage. Comparing Er^{3+} emission below or outside the graphene sheet as a function of the voltage applied to the device, it was possible to identify a regime of low emission in which Er^{3+} is quenched by the graphene, a stronger emission when

Table 1: Synthesis techniques and spectroscopic properties of Y_2O_3 (cubic phase) nanocrystals and films.

Dopants and topology	Object diameter/ thickness (nm)	Dopant concentration (at. %)	Synthesis method	Γ_{inh} (GHz)	T_1 (ms)	T_2 (µs)	Spin T_2 (ms)	Ref.
Eu^{3+}, nanocrystals	≈1000	0.9	Solvothermal	17	0.97	3.7		[64]
	400	0.3	Homogeneous precipitation	11	1.2	7	1.3, 8.1 (DD)	[80, 87]
	150	0.3	Homogeneous precipitation, chemical etching, post-processing	17		9.3		[82]
Eu^{3+}, films	100	5	ALD	200	0.8			[113]
	3000	2	CVD	90	0.9	0.03		[114]
Pr^{3+}, nanocrystals	150	0.05	Homogeneous precipitation, post-processing	27	0.14	1.0	0.88	[94]
Er^{3+}, films	7	2	ALD		1.5			[113]
	500	0.01	MBE	6.9	8.7			[117]

ALD, Atomic layer deposition; CVD, chemical vapor deposition; DD, dynamical decoupling; MBE, molecular beam epitaxy.

electron hole pair creation becomes reduced and finally a low emission again when Er^{3+} is able to excite plasmon in the graphene layer [62]. This demonstrates a unique capability of electrically controlling the local density of optical states of an emitter. The on-demand coupling of emitters with plasmons opens promising possibilities for quantum optoelectronics, which could take advantage of the coherence properties of rare-earth transitions. This will require large couplings that could be obtained with thinner films, provided that rare-earth properties can be preserved (see above, [113]).

A second example is the incorporation of rare-earth ions in diamond, one of the major materials for quantum technologies. Such a system could combine the excellent properties of diamonds such as high purity and crystalline quality with the narrow lines of rare-earth ions. Moreover, diamonds can host a variety of defects with strong emissions and/or carrying spins with long coherence lifetimes that could also interact with rare-earths in hybrid quantum systems. Incorporating rare-earth ions, which have a large ionic radius, into the diamond lattice is however difficult. One approach is to chemically self-assemble rare-earth complexes on bulk or nano-diamonds before growing a new diamond layer by CVD [122, 123]. Another one consists of implanting rare-earth into bulk or nano diamond [124, 125]. Rare-earth ion luminescence has been observed with these different methods, with long lifetimes in the case of Eu^{3+} ions [122]. The lack of well-resolved crystal field structure in the spectra, however, prevents a detailed analysis of the rare-earth local environment and comparison with simulations [122–124], which could unambiguously confirm their incorporation into diamonds, is still under debate [123]. High-resolution or coherent spectroscopy has not yet been reported on these systems. Meanwhile, there is also a large body of work on incorporation of Er ions in silicon [126–128], which has been proven successful for many classical optoelectronic applications. However, the similar lack of knowledge on the silicon crystal sites for Er has precluded further in-depth coherent spectroscopy, which is desired to enable quantum information applications of Er in silicon [129].

4 Outlook

Future advances in rare-earth nanophotonics hinge on breakthroughs in material synthesis, control and engineering. A set of material properties form the key metrics for guiding this material development and optimization. For nanocrystals, the particle size should be small enough for the precise localization of the emitter with respective to the optical field it couples to, while large enough to suppress unwanted decoherence due to proximity to particle surfaces. Taking the state-of-the-art photonic crystal resonators as an example, a nanoparticle size of approximately 100 nm would likely fulfil both requirements. For thin films, well controlled thickness and surface roughness (ideally with r.m.s. roughness much less than 1 nm) are important for high quality photonic devices. The dopant spectroscopic properties, including narrow optical and spin inhomogeneous linewidths, optical lifetimes, homogeneous linewidth, long spin T_1 and T_2, will continue to be the qualifying parameters that drive the growth optimization process. Some of these parameters are less restrictive than others for specific applications. For instance, for single ion devices, inhomogeneous broadening is of secondary concern as long as individual ions exhibit long-lived coherence. This is because the frequency of one ion can be readily tuned via the Stark effect or strain tuning to match a remote ion in the context of quantum network.

One decisively enabling capability for rare-earth nanophotonics is the deterministic control of doping concentration and placement in host matrices. The former is notoriously difficult in bulk, yttrium-based doped crystals, because the background doping of all sorts of trace rare-earth elements is at ppm level in the raw yttrium material. This limitation might be overcome with less common growth techniques such as floating zone growth or molecular beam epitaxy in which elements of rare-earths and yttrium can be better separated by their disparate vapor pressures or other physical properties, yielding a control of doping concentration at parts per billion (ppb) level. In terms of dopant placement, ALD and MBE offer powerful delta-doping options to precisely control the distance of dopant to material interfaces, and in principle could result in a mono layer thickness of the doped material. The mastery of 2D film growth technique will further spur new ways to control dopant placement in three-dimensional (3D), for instance, by combining delta-doping with aperture-masked doping at prescribed locations on the substrate. With nanocrystals containing one or a few rare-earth ions, their placement can be controlled by functionalizing the substrate surface and chemically docking the nanocrystal to the desired location.

Once the above metrics and capabilities are realized, they open up powerful tools to nanoscopically control and tailor interactions of rare-earth ions with other quantum degrees of freedoms. With regard to nanophotonics, such control will enable unprecedented enhancement of light-matter interaction at single rare-earth ion level,

and potentially unlock new coupling modalities such as rare-earth-phonon, rare-earth-electric field interactions at varying length and energy scales. Together, these new rare-earth materials and accompanying processing techniques present an exciting prospect of engineering highly coherent quantum systems with on-demand functionality and performance.

References

[1] Awschalom DD, Hanson R, Wrachtrup J, Zhou BB. Quantum technologies with optically interfaced solid-state spins. Nat Photonics 2018;12:516–27.

[2] Munro WJ, Azuma K, Tamaki K, Nemoto K. Inside quantum repeaters. IEEE J Selected Topics Quantum Electronics 2015;21:78–90.

[3] de Riedmatten H, Afzelius M. Quantum light storage in solid state atomic ensembles. In: Predojević MW, Michell A, editors. Engineering the atom-photon interaction. Cham, Switzerland: Springer, 2015:241–73.

[4] Hensen B, Bernien H, Dréau AE, et al. Loophole-free bell inequality violation using electron spins separated by 1.3 kilometres. Nature 2015;526:682.

[5] Degen CL, Reinhard F, Cappellaro P. Quantum sensing. Rev Mod Phys 2017;89:035002.

[6] DiVincenzo DP. The physical implementation of quantum computation. Fortschritte der Physik 2000;48:771–83.

[7] Kane BE. A silicon-based nuclear spin quantum computer. Nature 1998;393:133–7.

[8] Dutt MVG, Childress L, Jiang L, et al. Quantum register based on individual electronic and nuclear spin qubits in diamond. Science 2007;316:1312–6.

[9] Macfarlane RM. High-resolution laser spectroscopy of rare-earth doped insulators: a personal perspective. J Lumin 2002;100:1–20.

[10] Thiel C, Böttger T, Cone R. Rare-earth-doped materials for applications in quantum information storage and signal processing. J Lumin 2011;131:353–61.

[11] Tittel W, Afzelius M, Chanelière T, et al. Photon-echo quantum memory in solid state systems. Laser Photonics Rev 2010;4:244–67.

[12] Lvovsky AI, Sanders BC, Tittel W. Optical quantum memory. Nat Photonics 2009;3:706–14.

[13] Zhong T, Kindem JM, Bartholomew JG, et al. Optically addressing single rare-earth ions in a nanophotonic cavity. Phys Rev Lett 2018;121:183603.

[14] Dibos A, Raha M, Phenicie C, Thompson J. Atomic source of single photons in the telecom band. Phys Rev Lett 2018;120:243601.

[15] Brien CO, Lauk N, Blum S, Morigi G, Fleischhauer M. Interfacing superconducting qubits and telecom photons via a rare-earth-doped crystal. Phys Rev Lett 2014;113:063603.

[16] Williamson LA, Chen Y-H, Longdell JJ. Magneto-optic modulator with unit quantum efficiency. Phys Rev Lett 2014;113:203601.

[17] Goldner P, Ferrier A, Guillot-Noël O. Rare earth-doped crystals for quantum information processing. In: Bünzli J-CG, Pecharsky VK, editors. Handbook on the physics and chemistry of rare earths. Amsterdam: Elsevier, 2015:1–78.

[18] Sun Y, Thiel CW, Cone R, Equall R, Hutcheson R. Recent progress in developing new rare earth materials for hole burning and coherent transient applications. Proceedings of the Seventh International Meeting on Hole Burning, Single Molecules and Related Spectroscopies: Science and Applications. J Lumin 2002;98:281–7.

[19] Kunkel N, Goldner P. Recent Advances in rare earth doped inorganic crystalline materials for quantum information processing. Z Anorg Allg Chem 2018;644:66–76.

[20] Zhong M, Hedges MP, Ahlefeldt RL, et al. Optically addressable nuclear spins in a solid with a six-hour coherence time. Nature 2015;517:177–80.

[21] Rančić M, Hedges MP, Ahlefeldt RL, Sellars MJ. Coherence time of over a second in a telecom-compatible quantum memory storage material. Nat Phys 2017;14:50–4.

[22] Usmani I, Afzelius M, de Riedmatten H, Gisin N. Mapping multiple photonic qubits into and out of one solid-state atomic ensemble. Nat Commun 2010;1:12.

[23] Sinclair N, Saglamyurek E, Mallahzadeh H, et al. Spectral multiplexing for scalable quantum photonics using an atomic frequency comb quantum memory and feed-forward control. Phys Rev Lett 2014;113:053603.

[24] Longdell JJ, Fraval E, Sellars MJ, Manson NB. Stopped light with storage times greater than one second using electromagnetically induced transparency in a solid. Phys Rev Lett 2005;95:063601.

[25] Heinze G, Hubrich C, Halfmann T. Stopped light and image storage by electromagnetically induced transparency up to the regime of one minute. Phys Rev Lett 2013;111:033601.

[26] Clausen C, Usmani I, Bussières F, et al. Quantum storage of photonic entanglement in a crystal. Nature 2011;469:508–11.

[27] Bussières F, Clausen C, Tiranov A, et al. Quantum teleportation from a telecom-wavelength photon to a solid-state quantum memory. Nat Photon 2014;8:775–8.

[28] Saglamyurek E, Sinclair N, Jin J, et al. Broadband waveguide quantum memory for entangled photons. Nature 2011;469:512–5.

[29] de Riedmatten H, Afzelius M, Staudt MU, Simon C, Gisin N. A solid-state light–matter interface at the single-photon level. Nature 2008;456:773–7.

[30] Zhou Z-Q, Lin W-B, Yang M, Li C-F, Guo G-C. Realization of reliable solid-state quantum memory for photonic polarization qubit. Phys Rev Lett 2012;180:190505.

[31] Zhong T, Kindem JM, Bartholomew JG, et al. Nanophotonic rare-earth quantum memory with optically controlled retrieval. Science 2016;357:1392–5.

[32] Jobez P, Laplane C, Timoney N, et al. Coherent spin control at the quantum level in an ensemble-based optical memory. Phys Rev Lett 2015;114:230502.

[33] Longdell JJ, Sellars MJ. Demonstration of conditional quantum phase shift between ions in a solid. Phys Rev A 2004;69:032307.

[34] Hedges MP, Longdell JJ, Li Y, Sellars MJ. Efficient quantum memory for light. Nature 2010;465:1052–6.

[35] Afzelius M, Usmani I, Amari A, et al. Demonstration of atomic frequency comb memory for light with spin-wave storage. Phys Rev Lett 2010;104:040503.

[36] Sabooni M, Li Q, Kröll S, Rippe L. Efficient quantum memory using a weakly absorbing sample. Phys Rev Lett 2013;110:133604.

[37] Maring N, Farrera P, Kutluer K, Mazzera M, Heinze G, de Riedmatten H. Photonic quantum state transfer between a cold atomic gas and a crystal. Nature 2017;551:485–8.

[38] Wolfowicz G, Maier-Flaig H, Marino R, et al. Coherent storage of microwave excitations in rare earth nuclear spins. Phys Rev Lett 2015;114:170503.

[39] Probst S, Rotzinger H, Wünsch S, et al. Anisotropic rare-earth spin ensemble strongly coupled to a superconducting resonator. Phys Rev Lett 2013;110:157001.

[40] Dold G, Zollitsch CW, O'Sullivan J, et al. High-cooperativity coupling of a rare-earth spin ensemble to a superconducting resonator using yttrium orthosilicate as a substrate. Phys Rev Appl 2019;11:054082.

[41] Fernandez-Gonzalvo X, Chen Y-H, Yin C, Rogge S, Longdell JJ. Coherent frequency up-conversion of microwaves to the optical telecommunications band in an Er:YSO crystal. Phys Rev A 2015;6:062313.

[42] Fernandez-Gonzalvo X, Horvath SP, Chen Y-H, and Longdell JJ. Cavity-enhanced Raman heterodyne spectroscopy in Er^{3+}:Y_2SiO_5 for microwave to optical signal conversion. Phys Rev A 2019;100:033807.

[43] Kindem JM, Bartholomew JG, Woodburn PJT, et al. Characterization of $^{171}Yb^{3+}$:YVO_4 for photonic quantum technologies. Phys Rev B 2018;98:024404.

[44] McAuslan DL, Longdell JJ. Strong-coupling cavity QED using rare-earth-metal-ion dopants in monolithic resonators: what you can do with a weak oscillator. Phys Rev A 2009;80:062307.

[45] Brien CO, Zhong T, Faraon A, Simon C. Nondestructive photon detection using a single rare-earth ion coupled to a photonic cavity. Phys Rev A 2016;94:043807.

[46] Kolesov R, Xia K, Reuter R, et al. Optical detection of a single rare-earth ion in a crystal. Nat Commun 2012;3:1029.

[47] Utikal T, Eichhammer E, Petersen L, Renn A, Götzinger S, Sandoghdar V. Spectroscopic detection and state preparation of a single praseodymium ion in a crystal. Nat Commun 2014;5:3627.

[48] Nakamura I, Yoshihiro T, Inagawa H, Fujiyoshi S, Matsushita M. Spectroscopy of single Pr^{3+} ion in LaF_3 crystal at 1.5 K. Sci Rep 2014;4:7364.

[49] Kolesov R, Xia K, Reuter R, et al. Mapping spin coherence of a single rare-earth ion in a crystal onto a single photon polarization state. Phys Rev Lett 2013;111:120502.

[50] Siyushev P, Xia K, Reuter R, et al. Coherent properties of single rare-earth spin qubits. Nat Commun 2014;5:3895.

[51] Xia K, Kolesov R, Wang Y, et al. All-optical preparation of coherent dark states of a single rare earth ion spin in a crystal. Phys Rev Lett 2015;115:93602.

[52] Yin C, Rancic M, de Boo GG, et al. Optical addressing of an individual erbium ion in silicon. Nature 2013;497:91–5.

[53] Sinclair N, Oblak D, Thiel CW, Cone RL, Tittel W. Properties of a rare-earth-ion-doped waveguide at sub-kelvin temperatures for quantum signal processing. Phys Rev Lett 2017;118:100.

[54] Askarani MF, Puigibert MG, Lutz T, et al. Storage and reemission of heralded telecommunication-wavelength photons using a crystal waveguide. Phys Rev Appl 2019;11:054056.

[55] Corrielli G, Seri A, Mazzera M, Osellame R, de Riedmatten H. Integrated optical memory based on laser-written waveguides. Phys Rev Appl 2016;5:054013.

[56] Marzban S, Bartholomew JG, Madden S, Vu K, Sellars MJ. Observation of photon echoes from evanescently coupled rare-earth ions in a planar waveguide. Phys Rev Lett 2015;115:013601.

[57] Miyazono E, Craiciu I, Arbabi A, Zhong T, Faraon A. Coupling erbium dopants in yttrium orthosilicate to silicon photonic resonators and waveguides. Opt Express 2017;25:2863–71.

[58] Ding D, Pereira LMC, Bauters JF, et al. Multidimensional purcell effect in an ytterbium-doped ring resonator. Nat Photonics 2016;10:385–8.

[59] Zhong T, Kindem JM, Miyazono E, Faraon A. Nanophotonic coherent light-matter interfaces based on rare-earth doped crystals. Nat Commun 2015;6:8206.

[60] Zhong T, Rochman J, Kindem JM, Miyazono E, Faraon A. High quality factor nanophotonic resonators in bulk rare-earth doped crystals. Opt Express 2016;24:536–44.

[61] Zhong T, Kindem JM, Rochman J, Faraon A. Interfacing broadband photonic qubits to a cavity-protected rare-earth ensemble. Nat Commun 2017;8:14107.

[62] Tielrooij KJ, Orona L, Ferrier A, et al. Electrical control of optical emitter relaxation pathways enabled by graphene. Nat Phys 2015;11:281–7.

[63] Zhang H, Yang J, Gray S, et al. Transparent Er^{3+}-doped Y_2O_3 ceramics with long optical coherence lifetime. ACS Omega 2017;2:3739–44.

[64] Perrot A, Goldner P, Giaume D, et al. Narrow optical homogeneous linewidths in rare earth doped nanocrystals. Phys Rev Lett 2013;111:203601.

[65] Casabone B, Benedikter J, Hümmer T, et al. Cavity-enhanced spectroscopy of a few-ion ensemble in Eu^{3+}:Y_2O_3. New J Phys 2018;20:095006–9.

[66] Yang J, Quan Z, Kong D, Liu X, Lin J. Y2O3: Eu^{3+} microspheres: solvothermal synthesis and luminescence properties. Cryst Growth Des 2007;7:730–5.

[67] Abella ID, Kurnit NA, Hartmann SR. Photon echoes. Phys Rev 1966;141:391.

[68] Meltzer RS. Line broadening mechanisms and their measurement. In: Jacquier B, Liu G, editors. Spectroscopic properties of rare earths in optical materials. Berlin Heidelberg, Springer, 2005:191–265.

[69] Beaudoux F, Ferrier A, Guillot-Noël O, Chanelière T, Le Gouët J-L, Goldner P. Emission of photon echoes in a strongly scattering medium. Opt Express 2011;19:15236–43.

[70] Pierrat R, Carminati R, Le Gouët J-L. Photon echoes in strongly scattering media: a diagrammatic approach. Phys Rev A 2018;97:063816.

[71] Meltzer RS, Hong K. Electron-phonon interactions in insulating nanoparticles: Eu_2O_3. Phys Rev B 2000;61:3396–403.

[72] Sellars MJ, Meltzer RS, Fisk PTH, Manson NB. Time-resolved ultranarrow optical hole burning of a crystalline solid: Y_2O_3:Eu^{3+}. J Opt Soc Am B 1994;11:1468–73.

[73] Kunkel N, Bartholomew J, Welinski S, Ferrier A, Ikesue A, Goldner P. Dephasing mechanisms of optical transitions in rare-earth-doped transparent ceramics. Phys Rev B 2016;94:184301.

[74] Flinn GP, Jang KW, Ganem J, Jones ML, Meltzer RS, Macfarlane RM. Sample-dependent optical dephasing in bulk crystalline samples of Y_2O_3:Eu^{3+}. Phys Rev B 1994;49:5821.

[75] Zhang Y, Abraha A, Zhang R, et al. Luminescence properties of $caWO_4$ and $caWO_4$:Eu^{3+} nanostructures prepared at low temperature. Opt Mater 2018;84:115–22.

[76] Ramakrishna P, Rao TL, Singh A, Benarji B, Dash S. Structural and photoluminescence behavior of thermally stable Eu^{3+} activated $caWO_4$ nanophosphors via li$+$ incorporation. J Mol Struct 2017;1149:426–31.

[77] Sun L, Cao M, Wang Y, Sun G, Hu C. The synthesis and photoluminescent properties of calcium tungstate nanocrystals. J Crystal Growth 2006;289:231–5.

[78] Sohn S, Kwon Y, Kim Y, Kim D. Synthesis and characterization of near-monodisperse yttria particles by homogeneous precipitation method. Powder Technol 2004;142:136–53.

[79] de Oliveira Lima K, Rocha Gonçalves R, Giaume D, Ferrier A, Goldner P. Influence of defects on sub-Å optical linewidths in Eu^{3+}:Y_2O_3 particles. J Lumin 2015;168:276–82.

[80] Bartholomew JG, de Oliveira Lima K, Ferrier A, Goldner P. Optical line width broadening mechanisms at the 10 kHz level in Eu^{3+}:Y_2O_3 nanoparticles. Nano Lett 2017;17:778–87.

[81] Kim M, Mamin HJ, Sherwood MH, Ohno K, Awschalom DD, Rugar D. Decoherence of near-surface nitrogen-vacancy centers due to electric field noise. Phys Rev Lett 2015;115:087602.

[82] Liu S, Serrano D, Fossati A, Tallaire A, Ferrier A, Goldner P. Controlled size reduction of rare earth doped nanoparticles for optical quantum technologies. RSC Adv 2018;8: 37098–104.

[83] Walther A, Rippe L, Yan Y, et al. High-fidelity readout scheme for rare-earth solid-state quantum computing. Phys Rev A 2015;92:022319.

[84] Hartmann S. Photon, spin, Raman echoes. IEEE J Quantum Electron 1968;4:802–7.

[85] Ham BS, Shahriar MS, Kim MK, Hemmer PR. Spin coherence excitation and rephasing with optically shelved atoms. Phys Rev B 1998;58:11825–8.

[86] Guillot-Noël O, Goldner P, Beaudoux F, et al. Hyperfine structure and hyperfine coherent properties of praseodymium in single-crystalline $La_2(WO_4)_3$ by hole-burning and photon-echo techniques. Phys Rev B 2009;79:155119.

[87] Serrano D, Karlsson J, Fossati A, Ferrier A, Goldner P. All-optical control of long-lived nuclear spins in rare-earth doped nanoparticles. Nat Commun 2018;9:2127.

[88] Karlsson J, Kunkel N, Ikesue A, Ferrier A, Goldner P. Nuclear spin coherence properties of 151Eu3$+$ and $^{153}Eu^{3+}$ in a Y_2O_3 transparent ceramic. J Phys: Condens Matter 2017;29:125501.

[89] Longdell JJ, Alexander A, Sellars MJ. Characterization of the hyperfine interaction in europium-doped yttrium orthosilicate and europium chloride hexahydrate. Phys Rev B 2006;74:195101.

[90] Ahlefeldt RL, Zhong M, Bartholomew JG, Sellars MJ. Minimizing Zeeman sensitivity on optical and hyperfine transitions in $EuCl_3 6H_2O$ to extend coherence times. J Lumin 2013;143: 193–200.

[91] Cruzeiro EZ, Etesse J, Tiranov A, et al. Characterization of the hyperfine interaction of the excited $^5D_0$ state of Eu^{3+}:Y_2SiO_5. Phys Rev B 2018;97:094416.

[92] Macfarlane RM. Optical Stark spectroscopy of solids. J Lumin. 2007;125:156–74.

[93] Macfarlane RM, Arcangeli A, Ferrier A, Goldner P. Optical measurement of the effect of electric fields on the nuclear spin coherence of rare-earth ions in solids. Phys Rev Lett 2014;113:157603.

[94] Serrano D, Deshmukh C, Liu S, et al. Coherent optical and spin spectroscopy of nanoscale Pr^{3+}:Y_2O_3. 2019;arXiv:1909.02260.

[95] Fraval E, Sellars MJ, Longdell JJ. Method of extending hyperfine coherence times in Pr^{3+}:Y_2SiO_5. Phys Rev Lett. 2004;92:077601.

[96] Goldner P, Guillot-Noël O, Beaudoux F, et al. Long coherence lifetime and electromagnetically induced transparency in a highly-spin-concentrated solid. Phys Rev A 2009;79:033809.

[97] Guillot-Noël O, Le Du Y, Beaudoux F, et al. Calculation and analysis of hyperfine and quadrupole interactions in praseodymium-doped $La_2(WO_4)_3$. J. Lumin. 2010;130: 1557–65.

[98] Lovrić M, Glasenapp P, Suter D, et al. Hyperfine characterization and spin coherence lifetime extension in Pr^{3+}:$La_2(WO_4)_3$. Phys Rev B 2011;84:104417.

[99] Meltzer RS, Yen W, Zheng H, et al. Evidence for long-range interactions between rare-earth impurity ions in nanocrystals embedded in amorphous matrices with the two-level systems of the matrix. Phys Rev B 2001;64:100201.

[100] Eichhammer E, Utikal T, Götzinger S, Sandoghdar V. Spectroscopic detection of single Pr^{3+} ions on the $^3H_4$–$^1D_2$ transition. New J Phys 2015;17:1–7.

[101] Lutz T, Veissier L, Thiel CW, et al. Effects of fabrication methods on spin relaxation and crystallite quality in Tm-doped powders studied using spectral hole burning. Sci Technol Adv Mater 2016;17:63–70.

[102] Lutz T, Veissier L, Thiel CW, et al. Effects of mechanical processing and annealing on optical coherence properties of Er^{3+}:$LiNbO_3$ powders. J Lumin 2017;191:2–12.

[103] Ikesue A, Aung YL. Synthesis and performance of advanced ceramic lasers. J Am Ceram Soc 2006;89:1936–44.

[104] Ikesue A, Aung YL. Ceramic laser materials. Nat Photonics 2008;2:721–7.

[105] Liu S, Mares JA, Feng X, et al. Towards bright and fast $Lu_3Al_5O_{12}$:Ce,Mg optical ceramics scintillators. Adv Opt Mater 2016;4:731–9.

[106] Ferrier A, Thiel CW, Tumino B, et al. Narrow inhomogeneous and homogeneous optical linewidths in a rare earth doped transparent ceramic. Phys Rev B 2013;87:041102.

[107] Kunkel N, Ferrier A, Thiel CW, et al. Rare-earth doped transparent ceramics for spectral filtering and quantum information processing. APL Mater 2015;3:096103–7.

[108] Kunkel N, Bartholomew J, Binet L, Ikesue A, Goldner P. High-resolution optical line width measurements as a material characterization tool. J Phys Chem C 2016;120:13725–31.

[109] Alexander AL, Longdell JJ, Sellars MJ. Measurement of the ground-state hyperfine coherence time of $^{151}Eu^{3+}$:Y_2SiO_5. J Opt Soc Am B 2007;24:2479–82.

[110] Arcangeli A, Lovrić M, Tumino B, Ferrier A, Goldner P. Spectroscopy and coherence lifetime extension of hyperfine transitions in $^{151}Eu^{3+}$:Y_2SiO_5. Phys Rev B 2014;89:184305.

[111] Böttger T, Thiel CW, Sun Y, Cone RL. Optical decoherence and spectral diffusion at 1.5 μm in Er^{3+}:Y_2SiO_5 versus magnetic field, temperature, and Er^{3+} concentration. Phys Rev B 2006;73:075101.

[112] Miikkulainen V, Leskelä M, Ritala M, Puurunen RL. Crystallinity of inorganic films grown by atomic layer deposition: overview and general trends. J Appl Phys 2013;113:021301–102.

[113] Scarafagio M, Tallaire A, Tielrooij K-J, et al. Ultrathin Eu- and Er-doped Y_2O_3 films with optimized optical properties for quantum technologies. J Phys Chem C 2019;123:13354–64.

[114] Flinn G, Jang K, Ganem J, Jones M, Meltzer R, Macfarlane R. Anomalous optical dephasing in crystalline Y_2O_3:Eu^{3+}. J Lumin 1994;58:374–9.

[115] Guha S, Cartier E, Gribelyuk MA, Bojarczuk NA, Copel MC. Atomic beam deposition of lanthanum- and yttrium-based oxide thin films for gate dielectrics. Appl Phys Lett 2000;77:2710–2.

[116] Guha S, Bojarczuk NA, Narayanan V. Lattice-matched, epitaxial, silicon-insulating lanthanum yttrium oxide heterostructures. Appl Phys Lett 2002;80:766–8.

[117] Singh KAM, Rajh T, Zhong T, Guha S. Characterization of epitaxially grown erbium doped Y_2O_3 for quantum optics applications. In: Proceedings of APS March Meeting (Boston MA, USA), P11.00008, 2019.

[118] Reinemer GD. Optical characterization of perturbed sites in rare earth doped oxide crystals. PhD thesis, Montana State University, 2003.

[119] Boye D, Sun Y, Meltzer R, et al. Spectral hole burning of Eu^{2+} in MBE-grown superlattices of CaF_2:$Eu^{2+}CdF_2$. J Lumin 1997;72–74:290–1.

[120] Pang M, Lin J, Wang S, Yu M, Zhou Y, Han X. Luminescent properties of rare-earth-doped cawo4 phosphor films prepared by the pechini sol–gel process. J Phys: Condens Matter 2003;15:5157.

[121] Andriamiadamanana C, Ibanez A, Ferrier A, et al. Erbium-doped yttria thin films prepared by metal organic decomposition for up-conversion. Thin Solid Films 2013;537:42–8.

[122] Magyar A, Hu W, Shanley T, Flatté ME, Hu E, Aharonovich I. Synthesis of luminescent europium defectsin diamond. Nat Commun 2014;5:1–6.

[123] Vanpoucke DEP, Nicley SS, Raymakers J, Maes W, Haenen K. Can europium atoms form luminescent centres in diamond A combined theoretical-experimental study. Diam Relat Mat 2019;94:233–41.

[124] Cajzl J, Nekvindová P, Macková A, et al. Erbium ion implantation into diamond – measurement and modelling of the crystal structure. Phys Chem Chem Phys 2017;19:6233–45.

[125] Cajzl J, Akhetova B, Nekvindová P, et al. Co-implantation of Er and Yb ions into single-crystalline and nano-crystalline diamond. Surf Interface Anal 2018;5:3523–6.

[126] Vinh NQ, Ha NN, Gregorkiewicz T. Photonic properties of er-doped crystalline silicon. Proc IEEE 2009;97:1269–83.

[127] Polman A. Erbium implanted thin film photonic materials. J Appl Phys 1997;82:1–39.

[128] Kenyon AJ. Erbium in silicon. Semiconduct Sci Technol 2005;20:R65–84.

[129] Yin C, Rancic M, de Boo GG, et al. Optical addressing of an individual erbium ion in silicon. Nature 2013;497:91–4.